Reconstruction of tubular structures from 2.5D point clouds: A mesophotic gorgonian coral case study

F. Lupi[1]   S. J. Rowley[2]   M. Chyba[3]   M. Lanzetta[4]

Abstract

A method for the surface reconstruction of 3D tubular branched structures characterized by low informative point clouds (i.e., 2.5D) is proposed. These specific clouds can arise when using photogrammetry techniques on complex subjects in challenging scanning environments (e.g., underwater gorgonian coral at mesophotic depths). The core idea behind the proposed Sphere Skeleton Approach (SSA) is to approximate the assumed tubular shapes via merged spheres having variable radii and centered in the points of the medial skeleton. To assess the generality and robustness of the proposed SSA, additional experiments have been conducted on 2.5D point clouds that were synthetically generated from 3D model benchmarks. Hausdorff distances between the target and the

reconstructed 3D models are used to quantitatively compare the SSA performances to a classical meshing algorithm. Early results highlight the capability to outperform existing approaches in reconstructing objects from 2.5D clouds.

Contents

1   Introduction

Significant developments in Computer-Aided Design (CAD) have been achieved and three-dimensional (3D) digitization of physical objects has now been used proficiently in a wide array of fields [3]. In particular, applying 3D digitization methods to marine sessile organisms, such as corals in deep-reef environments, is an additional challenge that continually refines computational proficiency and helps us to understand growth patterns and responses to hydrodynamic forces. The motivation of this study is to present a solution to a problem that arose during the 3D reconstruction of a Indo-Pacific gorgonian coral, *Annella* Gray, 1858 (Cnidaria: Octorallia) (Figure 1).
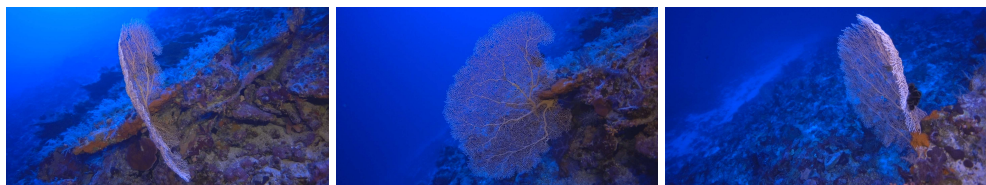
Figure 1: Three figures of the *Annella* coral; 60 meters depth, outer reef slope of Palikir Pass Marine Reserve, Pohnpei [12], Federated States of Micronesia.
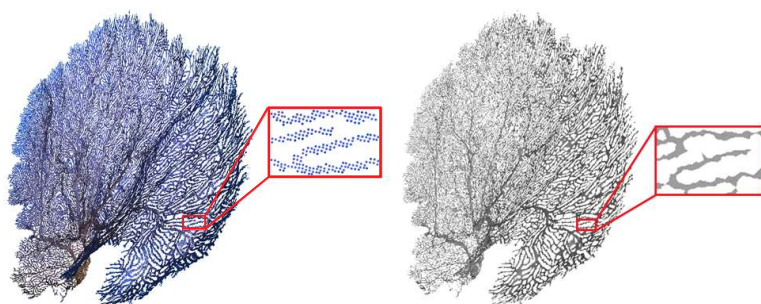

Figure 2: Isometric view of the *Annella* 2.5D point cloud with (left) 389 777 points and (right) unsatisfactory Metashape mesh reconstruction.

Due to the fragility of the corals and underwater environment, an in-situ contact-less approach was used (i.e., Structure-from-Motion (SfM) photogrammetry). After processing the 22 close-range underwater images of the *Annella* (Figure 1) into Agisoft Metashape Professional Edition, Version 1.5. [1], a 2.5D dense cloud was extracted (Figure 2, left). A 2.5D point cloud is defined as a cloud that belongs to an embedded surface in $\mathbb{R}^3$ whose atlas is composed of a single chart or patch. In other words, a 2.5D cloud Y can be obtained from a 2D cloud set that we denote by $\mathsf{X} \in \mathbb{R}^2$, through a bijective function $\mathsf{f} : \mathsf{X} \to \mathsf{Y}$.

Despite its flexibility, when discriminative point features are insufficient, SfM photogrammetry produces more challenging points clouds (e.g., 2.5D) to manage during the reconstruction process compared to more accurate

approaches (e.g., Laser Imaging Detection and Ranging (LiDAR) [3]). In the tubular 3D branched *Annella* coral case, for example, the 2.5D cloud could be a consequence of numerous unfavourable features of the subject (e.g., thinness, front-back symmetry and self-replication) as well as the challenging deep underwater conditions.

Unfortunately, there was a shortage of methods capable of reconstructing 2.5D point clouds when searching the literature or using commercial software. As shown in Figure 2 (right), the 2.5D point cloud is a source of serious issues in the final step of the Metashape [1] workflow (i.e., mesh generation). At a glance this causes huge distortion in the final model since the 3D volumetric tubular structure of the branches is completely missing.

The idea behind our contribution is to fill the gap in reconstructing 2.5D point clouds by retrieving two basic topological types of information from the subject stored in the 2.5D point cloud (i.e., radii and skeleton) to reconstruct the tubular 3D shape.

2   Skeleton-based reconstruction techniques

The method in this study is largely based on the results and ideas of skeleton-based approaches [3]. Among a broad spectrum of techniques we propose to use the "L-1 Medial Skeleton" algorithm [7], because of its capacity to deal with complex point clouds (e.g., 2.5D). As demonstrated by Mei et al. [11] a tree structure reconstruction from an incomplete point cloud was successfully achieved using the L-1 Medial Skeleton. Contrary to Mei et al. [11], we do not use an iterative optimization process to repair the regions of missing data. Instead, our proposed Sphere Skeleton Approach (SSA) approximates the cylindrical shapes by using techniques that address industrial pipe meshing problems [8] and using an adapted heuristic with particular relevance to the radii of the branches.

The idea of computing a skeleton and using it for reconstruction is also correlated to a remarkable work on wire object modeling [9]. In this work the

reconstruction of the complex point cloud of tubular objects was provided. However, no variable radius was accounted for and, therefore, is not applicable for our aim. Additional methodologies for tubular subjects reconstruction have been developed using skeleton-based reconstruction methods but none seem suitable for 2.5D clouds.

3   Proposed SSA method

3.1   Environment and equipment

Data was collected from the outer reef slope of Palikir Pass Marine Reserve, Pohnpei, Federated States of Micronesia (6 59030:000 N, 158 08013:100 E; Permit No.: MPA-0017). Underwater imagery of the gorgonian coral *Annella* (Figure 1) was conducted at 60 meters depth using mixed gas closed circuit rebreather diving technology (Divesoft Liberty CCR, with a Sony RX100MkV camera, INON UWL-H100 28M67 Type 2 wet lens, Nauticam NARX100V waterproof housing, and Sola light configuration. All field data were collected under the auspices of the British Sub-Aqua Club (BSAC; technical branch).

3.2   Skeleton points extraction from 2.5D cloud

As previously highlighted, after processing the underwater imagery of the *Annella* (Figure 1) into Metashape [1], a 2.5D dense cloud was extracted (Figure 2, left). From hereon, $\mathbf{P} = $ *point-set* $\in$ *Annella 2.5D point cloud* refers to the specific 2.5D point cloud from Figure 2 (left). The main steps of the adopted L-1 Medial Skeleton algorithm are as follows: (i) random selection of sample points from $\mathbf{P}$; (ii) iterative projection onto a skeletal point cloud with a gradually increasing neighborhood size; (iii) down-sampling, smoothing, and re-centering, in order to obtain the final central axis point cloud $\mathbf{S} = $ *point-set* $\in$ *Annella 2.5D point cloud skeleton*. Figure 3 graphically shows the skeleton point cloud extraction process.
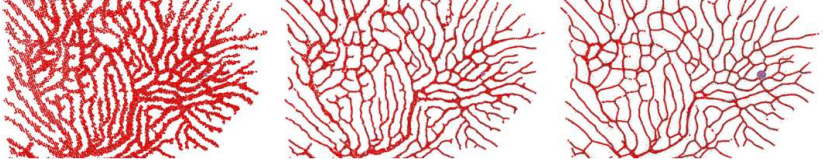
Figure 3: A close up view of **S** extraction adopting the algorithm presented by Huang et al. [7]. The panels show three consecutive steps from left to right: the initial condition, after ten iterations, and after ten more iterations.

Algorithm 1 SSA pseudo-code

 1: *Extract the point cloud skeleton* **S** *frrom* **P**
 2: *Define* r_0, k *and* $inc_\%$
 3: **for** *each* $point_j(x_j, y_j, z_j) \in$ **S** **do**
 4:     *Calculate the point density function*
 5:     *Evaluate the rules*
 6:     *Save the* r_j

 7: *Remove* r*-vector oversized outliers*
 8: **for** *each* $point_j(x_j, y_j, z_j) \in$ **S** **do**
 9:     *Mesh the sphere* j *with* r_j
10: *Merge all the spheres and post process*

3.3 Spheres construction

Algorithm 1 approximates the assumed tubular shape by the use of an heuristic that merges primitive geometries (i.e., spheres) whose centers are the points that belongs to **S** and the radii are detected using **P** as a reference.

Explanation of lines 1–6 (Algorithm 1):   After **S** (i.e., vector of spheres' centers) has been extracted (Section 3.2), define three parameters: (i) $r_0 =$ initial radius of the sphere; (ii) $k =$ number of iterations for the sphere radius increment; (iii) $inc_\% =$ percentage increment at each iteration. All the above parameters are defined by a heuristic approach (e.g., visual tests on **S** and **P**).

In the following step choose $r = r_0$ and let $q_j \in \mathbf{S}$. We construct the set: $N_{q_j}(r) = \{q_i \in \mathbf{P}, \|q_i - q_j\|_2^2 \leqslant r^2\}$. We introduce $n_{q_j} = \#N_{q_j}(r)$ the cardinal of set $N_{q_j}(r)$ and we define the PointDensity function for the skeleton point q_j as $f_j(r) = n_{q_j(r)}/r^2$. The process is iterative with k and $r = r_0(1 + \text{inc}_\%)^k$.

The idea behind the PointDensity function is to allow for automatic detection of changes using its qualitative behavior as the radius r varies. Under the assumption of sufficient and uniformly distributed data, a change in qualitative behavior can, for instance, signal that r might overcome the local size of the branch and the iteration process needs to be stopped.

In order to detect those changes, once the PointDensity function $f_j(r)$ is calculated for each iteration step k, the local maxima of $f_j(r)$ are identified and labeled (Figure 4, left). After that, a set of experimental rules have been developed as follows: (i) if no local maximum, then $r_j = r_{\max}$, where $r_{\max}$ is the upper bound after k iterations; (ii) if there is exactly one local maximum, then r_j is the radius corresponding to that local maximum; (iii) if the absolute maximum is attained at the lowest radius from the set of local maxima, then r_j is set as the radius of the second highest local maximum; (iv) else, r_j is set as the radius for which the PointDensity attains its absolute maximum.

Explanation of lines 7–10 (Algorithm 1):   To remove oversized radii, for each point $q_j \in \mathbf{S}$, select all the points in $\mathbf{S}$ whose spheres have $r_q < r_j$. We call the set formed by those points $\mathbf{S}_{q_j}$ and we denote by n_j its cardinality. Similarly, select all the points in $\mathbf{S}$ related to those spheres with a $r_q < 0.5r_j$. We call the set formed by those points $\mathbf{S}'_{q_j}$ and we denote by p_j its cardinality.

If the ratio between p_j and n_j is lower than a prescribed threshold (e.g., good experimental results suggested 90%), no changes need to be applied to r_j. Otherwise, we downsized the sphere by applying $r_j = \sum_{q \in s'_{q_j}} r_q/p_j$.

Convert the final 3D model to a mesh, merge the spheres and post-process. In this case, to address the intersections of the spheres, Boolean union were applied [6]. Figure 4 (right) shows the final reconstruction for the *Annella*.
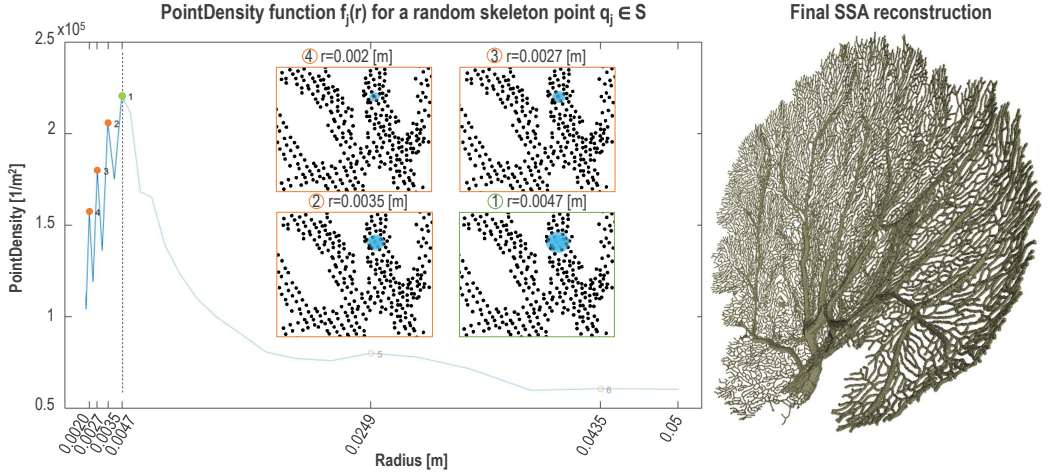
Figure 4: (Left) Local maxima sorted from the largest (i.e., first) to the smallest (i.e., sixth) and related close-up views of the sphere growth until the final r_j selection (i.e., dotted line and green window) for a random point q_j. (Right) Isometric view of the *Annella* SSA reconstruction.

4 Experimental benchmarking results

Due to the lack of a given 3D model and the incompleteness as well as distortion of the cloud data for the *Annella* case, a comparative analysis with respect to a reference was missing. To address this issue, the quality of SSA was measured on experimental examples where the given 3D models were known beforehand (Figure 5).

In particular, and motivated by the idea of synthetic scanning [2], we first simulated the 2.5D point clouds by extracting them from the ground-truth models, on which we then apply SSA for the 3D reconstruction. For the experiments we considered objects having structures quite close to the *Annella* (i.e., leaf and cactus Figure 5, first and second rows, respectively) and deliberately unrelated highly variable circular cross sections (i.e., dino Figure 5, third row).
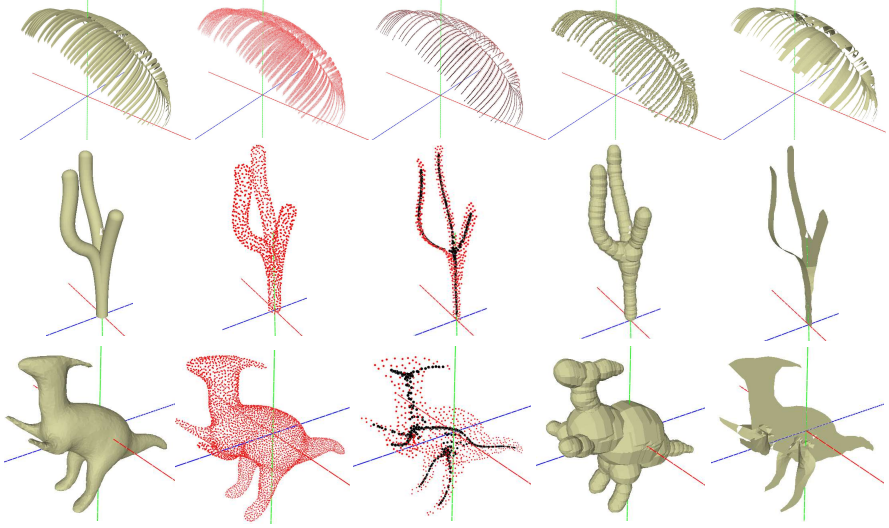
Figure 5: From left to right: given 3D mesh [14, 13]; synthetic 3D point cloud extracted from the envelope of the 3D structure; synthetic 2.5D point cloud (red) as a union of 2.5D clouds to retain the presence of the appendages of the 3D subjects and skeleton point cloud (black); SSA output using 2.5D point cloud as input; BPA output using 2.5D point cloud as input.

We then compared the outputs against the target meshes, computing the Hausdorff distance to represent the error, utilizing the algorithm implemented by Cignoni et al. [6]. This metric is calculated by sampling a collection of points over the surface of one of the two meshes (i.e., *sampled*), and finding for each sample the closest point over the other mesh (i.e., *reference*).

For a better assessment of our methodology, a classical interpolation technique (i.e., the Ball Pivoting Algorithm (BPA) [4]) implemented in Meshlab [6], was tested as well. We selected this algorithm as an arbitrary representative example among uncountable, less or more recent or advanced meshing algorithms, which are intrinsically unable to catch the 3D nature of the models from a 2.5D point cloud. Parameters adopted for SSA are shown in Table 1 (SSA

Table 1: Adopted SSA parameters and normalized Hausdorff distance for SSA and BPA. Note that RMS stands for Root Mean Square.

| Object | SSA parameters | | | Hausdorff distance | | |
	r_0	k	inc$_\%$	Mean% SSA-BPA	Max% SSA-BPA	RMS% SSA-BPA
Leaf	0.5	35	15	0.2–0.1	1.2–1.4	0.2–0.2
Cactus	0.003	20	14	0.7–2	3–4	0.8–2
Dino	0.01	30	15	0.3–3	6–9	0.6–4

parameters), while BPA adopted the default ones [6]. Aggregate statistics normalized with respect to the Bounding Box Diagonal (BBD) both for SSA and BPA are shown in Table 1 (Hausdorff distance).

5   Discussion and future developments

From Table 1 (Hausdorff distance) we deduce that our method approximates the target 3D models with a maximum error of approximately 6% BBD. Nonetheless, on average, the errors are almost in the 0.6% range. Looking qualitatively at Figure 5, it is evident that our method has outperformed the classical BPA methods for all of the experimental examples. The leaf model stands out due to having better results from the classical method for the given metrics but fails to reproduce the tubular 3D structure and, therefore, is not satisfactory.

Among the major limitations of the proposed SSA is the need for a tubular subject with a 2.5D point cloud. Moreover, the outputs from SSA are not perfectly accurate but do perform better than existing algorithms for this type of challenging 2.5D raw point cloud.

As for future developments, automated skeleton curves extraction from a 2.5D point cloud is still an open challenge in complex cases such as the *Annella* coral, and alternative algorithms could be considered. Implicit modeling (e.g.,

metaballs [5]) during the merging of spheres could reduce the post-processing step and this aspect deserves attention as well. More mathematically robust and general techniques such as topological data analysis is also ongoing [15]. The difficulty is that because of the irregular shape of the holes in between the branches within the *Annella* colony, it is unlikely that observing changes in homology would help determine the optimal radius. Nonetheless, implicit or prior knowledge related to self-repetitive fractal structures may help [10].

6   Conclusion

A Sphere Skeleton Approach (SSA) for automated surface reconstruction of 2.5D point clouds has been proposed assuming a tubular shape of the subject and approximating the surface by primitive geometries (i.e., spheres) centered in the skeleton points. A practical application of 2.5D biological point clouds has been presented from one of the most challenging scanning environments. An evaluation on a set of three synthetic 2.5D point clouds generated from benchmarks have been conducted as well.

The proposed SSA overcomes the problems of reconstructing 3D fine structures and captures the refined topology as closely as possible, starting from a low amount of information stored in the 2.5D point clouds. These lessons will help drive research in surface reconstruction and development of new software tools and algorithms for 2.5D point clouds.

References

[1] *Agisoft.* 2021. URL: https://www.agisoft.com/ (cit. on pp. C3, C4, C5).

[2] M. Berger, J. A. Levine, L. G. Nonato, G. Taubin, and C. T. Silva. "A benchmark for surface reconstruction". In: *ACM Trans. Graph.* 32.2 (2013), pp. 1–17. DOI: 10.1145/2451236.2451246 (cit. on p. C8).

[3] M. Berger, A. Tagliasacchi, L. M. Seversky, P. Alliez, G. Guennebaud, J. A. Levine, A. Sharf, and C. T. Silva. "A survey of surface reconstruction from point clouds". In: *Comput. Graph. Forum.* Vol. 36. 1. 2017, pp. 301–329. DOI: 10.1111/cgf.12802 (cit. on pp. C2, C4).

[4] F. Bernardini, J. Mittleman, H. Rushmeier, C. Silva, and G. Taubin. "The ball-pivoting algorithm for surface reconstruction". In: *IEEE Trans. Visual. Comput. Graph.* 5.4 (1999), pp. 349–359. DOI: 10.1109/2945.817351 (cit. on p. C9).

[5] J. F. Blinn. "A generalization of algebraic surface drawing". In: *ACM Trans. Graph.* 1.3 (1982), pp. 235–256. DOI: 10.1145/357306.357310 (cit. on p. C11).

[6] P. Cignoni, M. Callieri, M. Corsini, M. Dellepiane, F. Ganovelli, and G. Ranzuglia. "Meshlab: an open-source mesh processing tool". In: *Eurographics Italian Chapter Conference.* Ed. by V. Scarano, R. De Chiara, and U. Erra. 2008, pp. 129–136. DOI: 10.2312/LocalChapterEvents/ItalChap/ItalianChapConf2008/129-136 (cit. on pp. C7, C9, C10).

[7] H. Huang, S. Wu, D. Cohen-Or, M. Gong, H. Zhang, G. Li, and B. Chen. "L1-medial skeleton of point cloud." In: *ACM Trans. Graph.* 32.4 (2013), pp. 1–8. DOI: 10.1145/2461912.2461913 (cit. on pp. C4, C6).

[8] Y.-H. Jin and W.-H. Lee. "Fast cylinder shape matching using random sample consensus in large scale point cloud". In: *Appl. Sci.* 9.5 (2019), p. 974. DOI: 10.3390/app9050974 (cit. on p. C4).

[9] L. Liu, D. Ceylan, C. Lin, W. Wang, and N. J. Mitra. "Image-based reconstruction of wire art". In: *ACM Trans. Graph.* 36.4 (2017), pp. 1–11. DOI: 10.1145/3072959.3073682 (cit. on p. C4).

[10] B. B. Mandelbrot. *The fractal geometry of nature.* Vol. 1. W. H. Freeman New York, 1982. URL: https://www.nhbs.com/the-fractal-geometry-of-nature-book (cit. on p. C11).

[11] J. Mei, L. Zhang, S. Wu, Z. Wang, and L. Zhang. "3D tree modeling from incomplete point clouds via optimization and L_1-MST". In: *Int. J. Geo. Inf. Sci.* 31.5 (2017), pp. 999–1021. DOI: 10.1080/13658816.2016.1264075 (cit. on p. C4).

[12] S. J. Rowley, T. E. Roberts, R. R. Coleman, H. L. Spalding, E. Joseph, and M. K. L. Dorricott. "Pohnpei, Federated States of Micronesia". In: *Mesophotic Coral Ecosystems.* Springer, 2019, pp. 301–320. DOI: 10.1007/978-3-319-92735-0_17 (cit. on p. C3).

[13] K. Siddiqi, J. Zhang, D. Macrini, A. Shokoufandeh, S. Bouix, and S. Dickinson. "Retrieving articulated 3-D models using medial surfaces". In: *Machine Vis. Appl.* 19.4 (2008), pp. 261–275. DOI: 10.1007/s00138-007-0097-8 (cit. on p. C9).

[14] *Sketchfab.* 2021. URL: https://sketchfab.com/ (cit. on p. C9).

[15] L. Wasserman. "Topological data analysis". In: *Ann. Rev. Stat. Appl.* 5 (2018), pp. 501–532. DOI: 10.1146/annurev-statistics-031017-100045 (cit. on p. C11).

Author addresses

1. **F. Lupi**, University of Pisa, Department of Civil and Industrial Engineering, 56122 Pisa, ITALY.

mailto:francesco.lupi@phd.unipi.it
orcid:0000-0003-4994-0215

2. **S. J. Rowley**, University of Hawai'i at Mānoa, Department of Earth Science, POST 713B, 1680 East-West R,d. Honolulu, 96822, Hawai'i, USA.
mailto:srowley@hawaii.edu
orcid:0000-0001-9175-1106

3. **M. Chyba**, University of Hawai'i at Mānoa, Department of Mathematics, 2565 McCarthy Mall, Honolulu, 96822, Hawai'i, USA.
mailto:chyba@hawaii.edu
orcid:0000-0003-3379-3660

4. **M. Lanzetta**, University of Pisa, Department of Civil and Industrial Engineering, 56122 Pisa, ITALY.
mailto:lanzetta@unipi.it
orcid:0000-0002-1803-5717